Topics in Catalysis
https://doi.org/10.1007/s11244-020-01360-6

ORIGINAL PAPER

Layered Nanocomposite 2D-TiO_2 with Cu_2O Nanoparticles as an Efficient Photocatalyst for 4-Chlorophenol Degradation and Hydrogen Evolution

Matías Alegría[1] · Juan Aliaga[1] · Luis Ballesteros[2] · Clivia Sotomayor-Torres[3,4] · Guillermo González[5] · Eglantina Benavente[1,6]

Abstract
New composites formed by layered hybrid TiO_2(stearic acid) ($LHTiO_2$) and, Cu_2O nanoparticles were studied as photocatalysts that extend the response range to light visible for the evolution of hydrogen and the degradation of 4-chlorophenol. The results revealed that $LHTiO_2/Cu_2O$ exhibited a clearly improved photocatalytic degradation, about 5.6 times faster than pristine TiO_2, and hydrogen evolution of about 2.7 times higher than the TiO_2 anatase. The enhanced photocatalytic activity can be assigned to the properties of the two-dimensional morphology, in sheets-like arrangement of $LHTiO_2$, benefitting from the high exposure of surface, with more active sites available to improve matching with the surfaces of the Cu_2O nanocrystals and significant reduction of migration distances of photogenerated carriers. In the photocatalytic degradation, a mechanism Z-scheme is supported, and in the photocatalytic evolution of hydrogen a mechanism type II band alignment is indicated. Photocatalytic reuse tests showed that stability and catalytic activity of $LHTiO_2/Cu_2O$ were maintained for three cycles. Photoelectrochemical evaluation were performed through measurements of the photocurrent response and electrochemical impedance.

Keywords Layered 2D-TiO_2 · Cu_2O · Photocatalysis · Degradation of 4-chlorophenol · Hydrogen evolution

1 Introduction

Photocatalytic reaction systems have been extensively studied for environmental remediation and solar energy conversion [1–3]. Photocatalysis is a semiconductor-mediated process that can absorb and utilize light for chemical reactions, and requires semiconductors that can provide charge transfer to the surface-active sites, stability, and the harvesting of a wide range of the solar spectrum [4–6]. In this context, one of the most studied semiconductors is TiO_2, mainly for its low cost, low toxicity, photo-stability, reactivity and abundance [7, 8]. Nevertheless, its large bandgap (3.2 eV) and fast charge recombination limit its application in photocatalytic processes [9, 10].

Electronic supplementary material The online version of this article (https://doi.org/10.1007/s11244-020-01360-6) contains supplementary material, which is available to authorized users.

✉ Guillermo González
ggonzale@uchile.cl

✉ Eglantina Benavente
ebenaven@utem.cl

[1] Departamento de Química, Facultad de Ciencias Naturales, Matemáticas y del Medio Ambiente, Universidad Tecnológica Metropolitana, Santiago, Chile

[2] Instituto de Ciencias Químicas Aplicadas, Inorganic Chemistry and Molecular Material Center, Facultad de Ingeniería, Universidad Autónoma de Chile, El Llano Subercaseaux, 2801 San Miguel, Santiago, Chile

[3] Catalan Institute of Nanoscience and Nanotechnology (ICN2) CSIC and BIST, Campus UAB Bellaterra, 08193 Barcelona, Spain

[4] ICREA, Pg. Lluís Companys 23, 08010 Barcelona, Spain

[5] Departamento de Química, Facultad de Ciencias, Universidad de Chile, Las Palmeras, 3425 Santiago, Chile

[6] Programa Institucional de Fomento a la Investigación, Desarrollo e Innovación (PIDi), Universidad Tecnológica Metropolitana, Santiago, Chile

Published online: 01 September 2020

An effective approach to design efficient photocatalysts is the strategy of coupling a TiO_2 wide-band-gap semiconductor with narrow-band-gap semiconductors, such as Cu_2O [11–14], RuO_2 [15] and CdS [16, 17], amongst others, broadens the absorption range and can also show superior photocatalytic performance because of the charge transfer between the two different types of semiconductors. This decreases the electron/hole recombination, while maintaining good compatibility between the two semiconductors, increase the matching of the semiconductors bandgap, with the essential feature of using the hole oxidation power for the degradation of water pollutants and the electron reduction power for the evolution of hydrogen [8, 18].

Among these materials, Cu_2O has emerged as the right candidate. It is a p-type semiconductor, abundant and low-cost, with a direct bandgap of 2.0 eV, which can be excited by visible light [19–21]. Some reports indicate that a drawback in Cu_2O photocatalysts lies in their poor stability under irradiation [22]. However, the reduction in situ of Cu^+ to Cu of Cu_2O after photoexcitation provides mobility of the electronic charge and does not slow down the process of photocatalysis [23, 24].

From the studies reported, n-type TiO_2 coupling with p-type Cu_2O exhibits good prospects for photocatalytic applications under visible light. For example, it was used in different applications such as the removal of organic and inorganic pollutants [20, 25–28], CO_2 reduction [29, 30], H_2 evolution [14, 31–33], polyester textiles [34], as well as for antibacterial activity [35, 36].

Herein, in this work, we report a photoactive material formed by layered hybrid TiO_2(stearic acid), ($LHTiO_2$), obtained by "bottom-up" methods using stearic acid as a template, following sol–gel procedures designed for the formation of TiO_2. The material possesses a sheet-like arrangement intercalated between self-assembled carboxylic acid monolayers, which gives properties as a two-dimensional (2D) material. The morphology of a semiconductor performs a crucial role in defining its photocatalytic activity. Thus, 2D material with a sizable interfacial contact area, to increase sunlight collection and the absorbent capacity of its organic components, combined with a narrow-band semiconductor, such as Cu_2O cubic nanoparticles, that extend the absorption range, achieve optimum performance in both photocatalytic processes. Photocatalytic degradation of 4-chlorophenol (4-CP) and evolution H_2 mechanisms studied corroborates the synergy between both semiconductors. In addition, $LHTiO_2/Cu_2O$ catalytic reuse tests show the presence of a minor proportion of Cu, however the stability and catalytic activity of $LHTiO_2/Cu_2O$ was retained for three cycles. We also complement the study by electrochemical impedance spectroscopy (EIS) and measurement efficiency of photocurrent conversion.

2 Experimental Section

2.1 Materials and Reagents

All chemical reagents used were obtained from commercial sources as guaranteed grade reagents. $Ti[OCH(CH_3)_2]_4$ (titanium tetraisopropoxide), $C_{18}H_{36}O_2$ (stearic acid), $C_6H_8O_6$ (ascorbic acid) and N_2H_4 (hydrazine) were purchased from Sigma-Aldrich. Methanol, ethanol and 4-Chlorophenol (4-CP) were purchased from Merck.

2.2 Preparation

2.2.1 Layered Hybrid Titanium Nanocomposite ($LHTiO_2$)

This was synthesized following a procedure described in the literature [16]. Elemental analysis for $TiO_2(C_{18}H_{35}O_2)_{1.3} \times 0.7\ H_2O \times 0.1(C_{18}H_{35}O_2)$ was: Calc. (%): C, 61.96; H, 10.04. Found (%): C, 61.98; H, 10.00; TiO_2: 15.80 (calculated based on thermogravimetric analysis Fig S1).

2.2.2 Cu_2O Nanoparticles

The nanoparticles were synthesized following a procedure described in the literature [37]. The solid obtained was washed and oven-dried at 45 °C for 24 h.

2.2.3 $LHTiO_2/Cu_2O$ Composites

The samples were mixed mechanically in an agate mortar (relation w/w). Before irradiation, the suspension was ultrasonicated for 2 min to produce a homogeneous sample, facilitating close contact and minimizing aggregation.

2.3 Characterization Methods

X-ray diffraction (XRD) analyses of the products were performed using a Bruker D8 Advance (Cu Kα λ = 1.5418 Å). The images of scanning electron microscopy (SEM) were obtained using a Quanta FEG250 and EVO MA 10 ZEISS microscope. X-ray photoelectron spectra (XPS) were obtained in a STAIB system with an RQ-300 X-Ray source using monochromated Al Kα X-rays (1486.6 eV, 75 W). The UV–vis diffuse reflectance spectra (DRS) were recorded in the range of 200–800 nm using a UV–Vis Shimadzu double beam (model 2450 PC) spectrometer. Reflectance measurements were converted to absorption spectra using the Kubelka–Munk function. Thermogravimetric analyses were recorded in a TG/DSC 1100 SF Mettler Toledo. Photoluminescence (PL) spectra were recorded in a fluorescence spectrophotometer (PerkinElmer, model LS 55). Ultraviolet–visible spectra were recorded at room temperature in

a UV–vis spectrometer (Jasco, model V-730). Nitrogen adsorption/desorption isotherm studies were achieved with Quantachrome Instruments (Nova 2200e, USA) using the Brunauer–Emmett–Teller (BET) method to determine the surface area. The samples were degassed at 50 °C for $LHTiO_2$ and 200 °C for TiO_2, 12 h prior to the measurements. The average pore size was measured according to the Barret–Joyner–Halenda (BJH) method. Analysis of particle size distribution by dynamic light scattering (DLS) was performed with a zetasizer NanoZS90 Malvern.

2.4 Measurement of Photocatalytic Activity and Hydroxyl Radicals

2.4.1 Photocatalytic Degradation

The photocatalytic activities of the nanocomposites were studied in visible light irradiation by testing the degradation of 4-CP as a pollutant. For this study, the characteristic absorption peaks of this compound, as an aqueous solution, were examined at regular intervals at 280 and 225 nm using a UV–Vis spectrophotometer. The effect of the initial content of the 4-CP solutions was examined at different concentrations: 1×10^{-5} M, 1×10^{-4} M and 5×10^{-5} M, in the pH range 6–7. According to the experimental findings, the best result in the degradation of 4-CP was the concentration of 5×10^{-5} M. The photocatalytic experiments were therefore carried out by mixing 10 mg of $LHTiO_2$, with different proportions of Cu_2O nanoparticles in 25 mL of a 5×10^{-5} M solution at pH 7.0. Before the measurements, the suspension was maintained in the dark for 30 min to reach an adsorption/desorption equilibrium. Instead of sunlight, the suspensions were irradiated by a solar simulator (Sciencetech SS 150 W) equipped with a 150 W ozone-free xenon bulb that produced a spectrum at an intensity of 1000 W/m^2 (1 sun). All samples were under constant magnetic stirring to guarantee a high level of homogeneity of the photocatalyst in the suspension. Approximately 0.35 mL of the reaction mixture was taken out at different times and centrifuged to avoid light scattering due to the interference from the suspended catalyst particles. The 4-CP concentration after equilibration was considered as the initial concentration (C_0) and was monitored in the UV–vis spectra of the solution using nanopure water as a reference.

2.4.2 Photocatalytic H_2 Generation

The photocatalytic activities were evaluated by H_2 production. The photocatalyst H_2 generation activity was tested in a Schlenk tube of 50 mL equipped with an inert gas supply with a dual-stage regulator, under direct light of the photocatalyst, dispersed in 20 mL of 20 vol% methanol solution. In a typical process, the reaction suspension was evacuated and purged with N_2 gas three times, for the removal of dissolved gases. The reactor was irradiated with a 300 W Xe arc lamp (Newport) under magnetic stirring, and the gas evolved during the reaction process was collected using the water displacement technique. Gas aliquots of 0.5 cm^3 were taken and analysed with a Shimadzu GC-2014 using a 5 Å molecular sieve column and a thermal conductivity detector (TCD).

2.4.3 Hydroxyl Radicals

During the photocatalytic reactions, active $^{\cdot}OH$ radicals were detected by the PL method, using terephthalic acid (TA) 4 mM in an alkaline medium (pH 8). TA reacts with $^{\cdot}OH$ and generates a highly fluorescent product, 2-hydroxyterephthalic acid (TAOH) [38]. Every 10 min after UV irradiation, a small amount of reaction solution was centrifuged and analysed in a spectrofluorometer. The total UV irradiation time was 90 min. The fluorescence product was detected as an emission peak at the maximum wavelength of 426 nm, with an excitation wavelength of 325 nm.

2.5 Electrochemical Measurements

All photoelectrochemical measurements were performed with a Zahner Zennium Electrochemical Workstation PP211. Cu_2O, $LHTiO_2$ and $LHTiO_2/Cu_2O$ (1:0.1) electrodes were used as photoelectrodes, platinum as counter electrode and Ag/AgCl (3 M NaCl, 0.205 V vs. NHE) as reference electrode. The electrodes were exposed to illumination in 0.5 M Na_2SO_4. A LED $\lambda = 365$ nm (50 W m^{-2}) was used for irradiation. To prepare the working electrode, FTO (fluorine-doped tin oxide) glass was ultrasonically cleaned, first with distilled water and then with acetone. We then prepared a thin film of sample on FTO glass by drop-casting a homogeneous ink of sample dispersed in ethylene glycol, controlling the area of 1.0 cm^2. Potential pulse measurements were taken at a 0 V bias vs. Ag/AgCl reference electrode with a pulse of 20 s under intermittent irradiation. EIS and photoelectrochemical impedance spectroscopy (PEIS) measurements were carried out in the frequency range of 100 MHz–10 kHz with an applied voltage signal of 0 V vs. reference electrode and ac amplitude voltage of 10 mV.

3 Results and Discussion

The synthetic route to $LHTiO_2/Cu_2O$ was illustrated in Scheme 1. X-ray diffraction (XRD) analyses of the products was used to study the structure, Fig. 1 shows the XRD patterns of the synthesized $LHTiO_2$, Cu_2O, and $LHTiO_2/Cu_2O$ nanocomposites. The pattern of $LHTiO_2$ shows a series of equidistant Bragg reflections at low 2-theta angles,

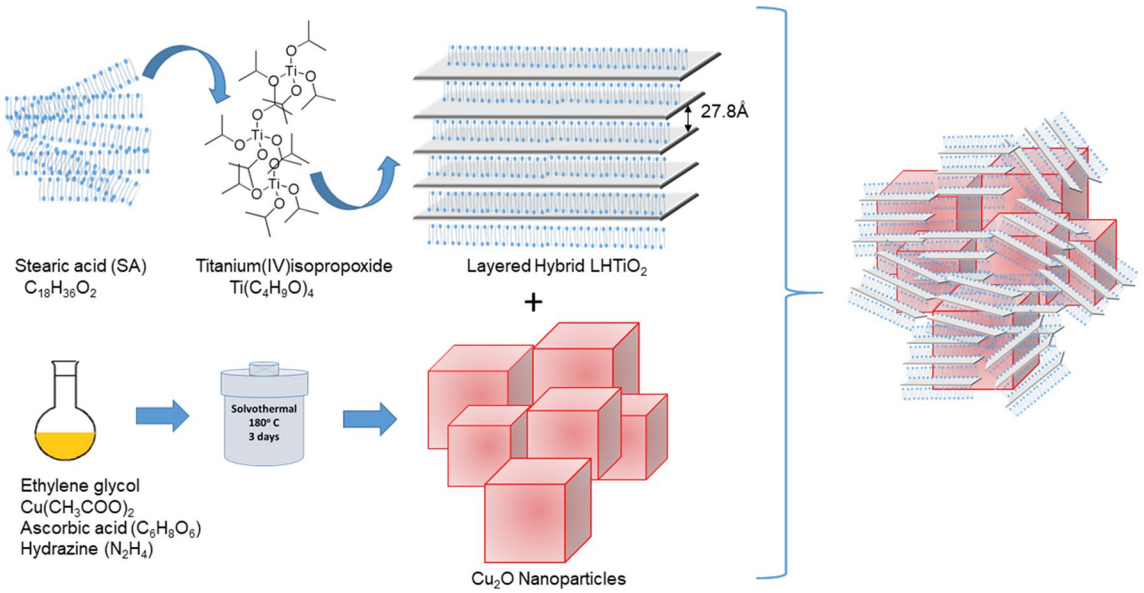

Scheme 1 Schematic illustration of synthetic routes for nanocomposite $LHTiO_2/Cu_2O$

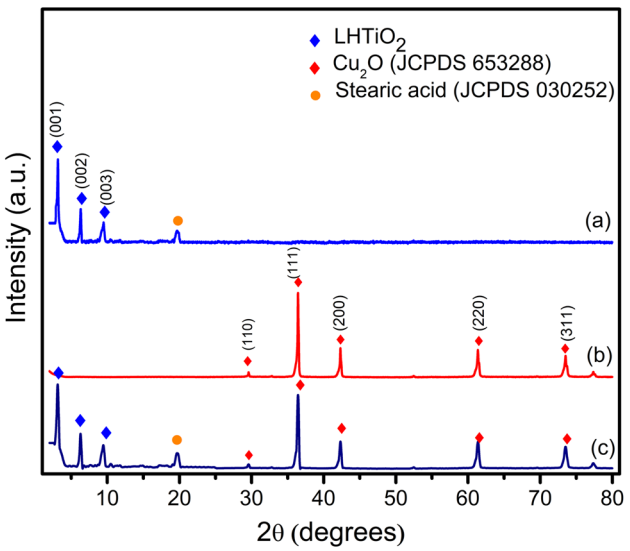

Fig. 1 XRD patterns of **a** $LHTiO_2$; **b** Cu_2O and **c** $LHTiO_2/Cu_2O$ (1:0.1)

characteristic of an ordered layered arrangement. The diffraction peaks at 2θ values of 3.19°, 6.52° and 9.47° are in good agreement with the first three (00l) reflections in a lamellar solid with a basal-distance along the c-axis of 27.8 Å. The low intensity peaks at 19.7° may be ascribed to a small excess of free stearic acid (JCPDS 03-0252). The XRD results confirm the lamellar nature of $LHTiO_2$, constituted by a layer of semiconductor scattered among self-assembled carboxylic acid molecules [16]. This structure is also retained in the composite $LiHTiO_2/Cu_2O$. Moreover, in Fig. 1, the XRD patterns indicate that the product is a material consisting of layered hybrid $LHTiO_2$ and Cu_2O nanoparticles. The main facets (111), (200), (220) and (311) of the Cu_2O cubic phase (JCPDS 65-3288) appeared at 2θ = 36.42°, 42.30°, 61.52° and 73.70°, respectively, and no impurities were apparent in the material.

Scanning electron microscopy (SEM) was used to examine the morphology and microstructure of the samples produced. Figure 2a shows the morphology of a conventional 2D $LHTiO_2$ sample. The AFM image Fig. 2b shows that the sample surface is stepped with steps of approx. 3 mn high. This characteristic is consistent with the width of a single layer of $LHTiO_2$, 2.78 nm (Fig. 1), as well as with the average thickness of micrometer particles of material of ~ 18 nm, as estimated by the Scherrer equation, corresponding to about 6 single hybrid layers per particle [16]. Figure 2c shows the very regular cubic Cu_2O nanoparticles of 60 nm (particle diameter measured by dynamic light scattering (DLS) in Fig S2). Figure 2d illustrates the morphology of the $LHTiO_2/Cu_2O$, where a combination of the structures, such as layers of $LHTiO_2$ and cubes of Cu_2O nanoparticles, can be seen. Figure 2e shows the energy dispersive X-ray spectroscopy (EDX) pattern, confirming the presence of Ti and Cu in the composite. EDX elemental mapping of $LHTiO_2/Cu_2O$ provides the dominant distribution of Ti and less dense regions of Cu in the nanostructure (Fig. S3).

Diffuse reflectance spectroscopy (DRS) was employed to characterize the samples. The absorbed light wavelength distribution is directly influenced by their electronic bandgap structure, which determines the photocatalytic activity of the materials. Figure 3a shows the UV–vis DRS of $LHTiO_2$,

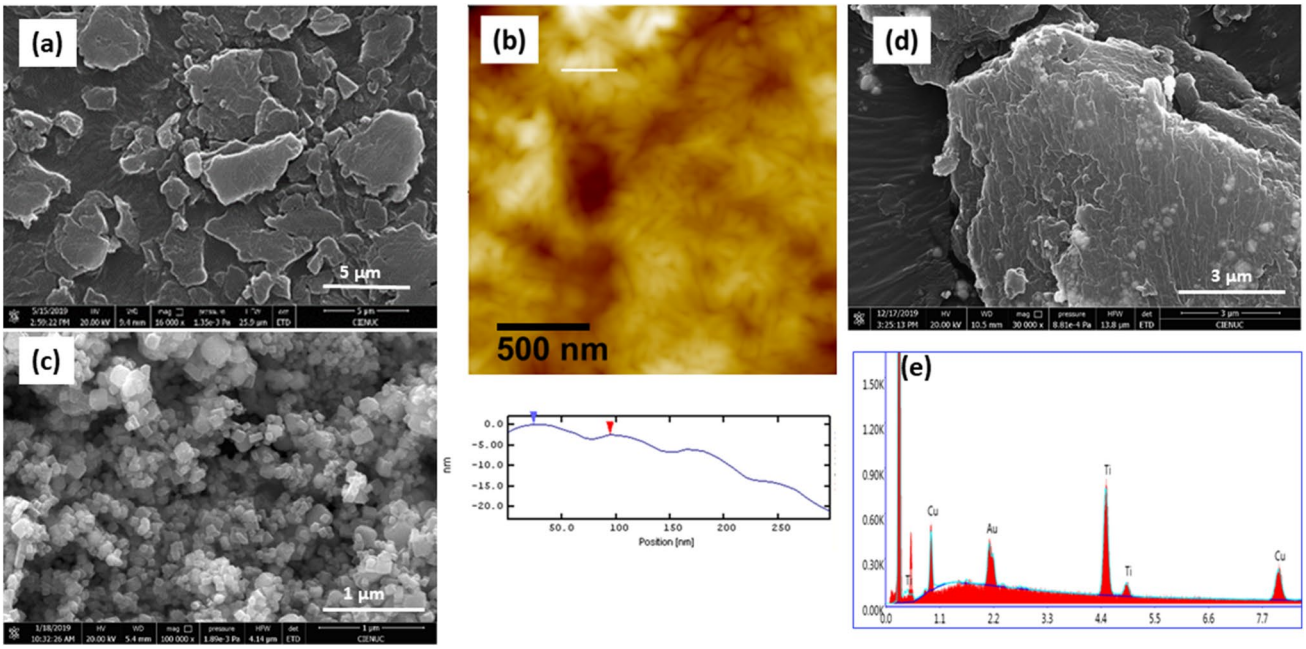

Fig. 2 **a** SEM images of $LHTiO_2$; **b** AFM images of $LHTiO_2$; **c** SEM images of Cu_2O cubic nanoparticles; **d** SEM images of $LHTiO_2/Cu_2O$ composite and **e** EDX pattern of $LHTiO_2/Cu_2O$ composite

Cu_2O, and the $LHTiO_2/Cu_2O$ composite. A sharp fundamental absorbance edge for $LHTiO_2$ was observed at 378 nm, exhibiting a wide bandgap of 3.28 eV. Cu_2O can absorb a certain wavelength range of visible light of 530 nm, with a forbidden bandwidth of 2.34 eV. The bandgap of the samples was analysed using the Tauc method. The energy (Eg), estimated from a plot of $(\alpha h\upsilon)^2$ versus the photon energy and the intercept of a tangent to the x-axis, was recorded. As shown in the insert, E_g were determined from the spectra [39, 40]. The results reveal that the combination of catalysts presents a broad absorbance in the UV and visible range, demonstrating that the composite $LHTiO_2/Cu_2O$ may allow more visible light absorption, thus improving its photocatalytic behavior [25, 41].

Photoluminescence (PL) emission spectra were used to appreciate the separation of the photoinduced electrons and holes in the samples and understand the transitions involved of the PL bands. Figure 3b shows the typical PL spectra of $LHTiO_2$ and $LHTiO_2/Cu_2O$ in the wavelength range of 360–550 nm. For the assignment of the peaks, a Gaussian adjustment was used in the PL spectra. The emission peaks at 380 nm is attributed to the band PL phenomenon, of the energy bandgap of anatase, the emission peak at 490 nm is ascribed to the excitation in the titanium states of $LHTiO_2$, and the signal at 533 nm is assigned to the oxygen vacancies [13, 42]. The luminescence intensities for the $LHTiO_2/Cu_2O$ photocatalyst is lower than $LHTiO_2$, indicating a low recombination and thus better charge carrier life-time [43].

XPS was utilized to analyse the composition and chemical state of Cu, Ti and O in Cu_2O, and $LHTiO_2$. In Fig. 4a, the Cu 2p3/2 and Cu 2p1/2 binding energy appeared at 932.5 eV and 952.2 eV, respectively, confirming the presence of the Cu^+ characteristic peak of Cu_2O [44]. Meanwhile, the satellite peaks of the Cu 2p1/2 and Cu 2p3/2 binding modes of the Cu and Cu^{+2} are not detected [23]. In Fig. 4b, the characteristic peak of anatase TiO_2 was observed at the binding energy of Ti 2p3/2 and Ti 2p1/2, respectively, at 458.7 eV and 464.2 eV. The binding energies of the Cu and Ti modes are in good accord with those of prior reports [32, 43, 44]. XPS of O1s spectra are presented in Fig. S4. The XPS results indicate that the Cu^+, Ti^{+4} and O^{-2} states exist in the initial sample at the beginning of the photocatalysis studies. The XPS spectra of the sample with the composite of $LHTiO_2/Cu_2O$ have been difficult to interpret due to the changes in copper, and the charge correction in the adventitious carbon being influenced by the organic surfactant. According to literature we assigned the peak of 930 eV as an artefact for the adjustment of C1s [45, 46]. (Fig S4).

The results of the porosity analysis and the surface properties obtained by BET of TiO_2 and $LHTiO_2$ are shown in Fig. 5. The pore size calculated using the BJH method was approximately 2.897 nm and 4.102 nm (inset in Fig. 5) for TiO_2 and $LHTiO_2$, respectively. The BET surface area was 10.468 m^2g^{-1} for TiO_2 and 37.428 m^2 g^{-1} for $LHTiO_2$. The isotherms exhibit a similar type II curve for TiO_2, which shows the non-porous nature of the TiO_2 nanoparticles [47], and for the $LHTiO_2$ sample, the isotherm showed a type IV

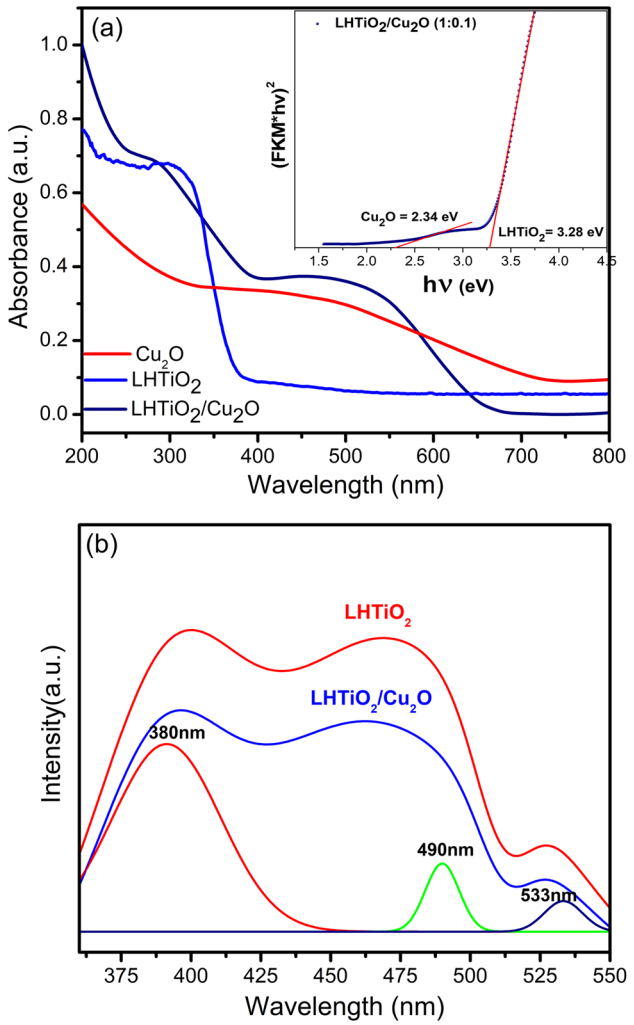

Fig. 3 **a** UV–vis diffuse reflectance spectra of Cu_2O, $LHTiO_2$ and $LHTiO_2/Cu_2O$ (1:0.1). The insert is the Tauc plots of $LHTiO_2/Cu_2O$ (1:0.1); **b** Photoluminescence (PL) emission spectra of $LHTiO_2$ and $LHTiO_2/Cu_2O$ (1:0.1)

curve with a type H3 hysteresis loop, which correlated with aggregates of platelike particles, characteristic of layered nanocomposites [48, 49]. In addition, the increase in the specific surface area in $LHTiO_2$ is 3.7 times greater than the TiO_2, which significantly improves photocatalytic properties, providing more surface-active sites as a 2D material.

3.1 Photocatalytic Activity

The photocatalytic activity of the $LHTiO_2/Cu_2O$ nanocomposites was studied by testing the degradation of 4-CP as a pollutant with different irradiation times under sunlight. Figure 6a shows the dye degradation in the presence of $LHTiO_2/Cu_2O$ composites with $LHTiO_2$ molar ratios of 1:0.05, 1:0.1 and 1:0.2, comparing them to those of the Cu_2O and $LHTiO_2$ separately. No photocatalytic activity was perceived in the control sample of 4-CP under irradiation. Both the Cu_2O nanoparticles alone and $LHTiO_2$ composite show an inferior photocatalytic behaviour compared to the $LHTiO_2/Cu_2O$ composites. The photocatalytic activity of the $LHTiO_2/Cu_2O$ (1:0.2) compound does not show a significant change with the performance of the $LHTiO_2/Cu_2O$ (1:0.1) compound, possibly due to the opacity of the sample, excess Cu_2O covers the surface active sites of the $LHTiO_2$, thus hindering light absorption [49]. Therefore, the optimal ratio for the $LHTiO_2/Cu_2O$ of 1:0.1 was selected. Indeed, as observed in Fig. 6a, the photocatalytic efficiency of $LHTiO_2/Cu_2O$ (1:0.1) after 300 min of irradiation was about 73.3%, which is significantly higher than that of $LHTiO_2$ at 43.9%, whereas only 3% degradation was observed without catalyst. Figure 6b illustrates the changes in the UV–visible absorption spectra of 4-CP at different irradiation times. 4-CP has strong absorption bands at wavelengths of 223 and 278 nm. As the reaction develops, the characteristic peaks gradually decrease as the reaction mixture is exposed to the irradiation [50].

The photocatalytic properties of the samples were evaluated under comparable conditions. All the curves were normalized after allowing the suspension to reach adsorption/desorption equilibrium in the dark. For a better understanding of the photocatalytic efficiency of the catalysts, the kinetic analysis of the photocatalytic degradations, shown in Fig. 6c can be described by a pseudo-first-order kinetics, with $\ln(C_0/C) = kt$, where k is the corresponding kinetic constant, and t is the irradiation time. The apparent rate constant (k_{app}, min^{-1}) of the $LHTiO_2/Cu_2O$ (1:0.1) nanocomposite is about 5.6 times faster than that of the TiO_2 anatase. The photocatalytic performance observed in the composites in visible light validates the synergistic effects mentioned above. The better photocatalytic performance of $LHTiO_2/Cu_2O$ (1:0.1) could be ascribed to the lower recombination of the photo-generated electrons and holes and a greater close interface between the 2D sheets with the flat surfaces of the Cu_2O. Besides, the presence of a hydrophobic organic moiety in $LHTiO_2$ contributes significantly to the photocatalytic increase, previously observed in photocatalytic studies of organo-inorganic hybrids of TiO_2 and ZnO [16, 37].

3.2 Proposed Degradation Mechanism

To further investigate the probable mechanistic effects associated with the role of the composites, we performed experiments aiming to detect the radical species involved in the 4-CP photodegradation using particular radical scavengers. For these experiments, we used oxalate of ammonium (OA) as a hole (h^+) scavenger, isopropanol (IPA) as an $^{\cdot}OH$ scavenger, and benzoquinone (BQ) as an $^{\cdot}O_2^-$ scavenger, at concentrations of 1 mmol [51]. Specifically, we tested the 4-CP degradation rate in the presence of each of the scavengers,

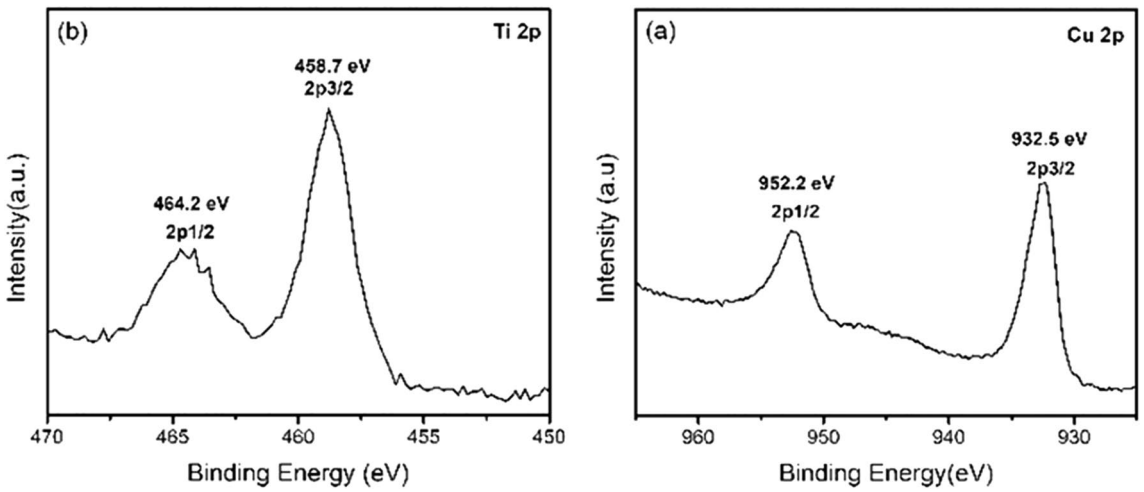

Fig. 4 High resolution spectra of **a** Cu 2p XPS spectra of Cu_2O; **b** Ti 2p XPS spectra of $LHTiO_2$

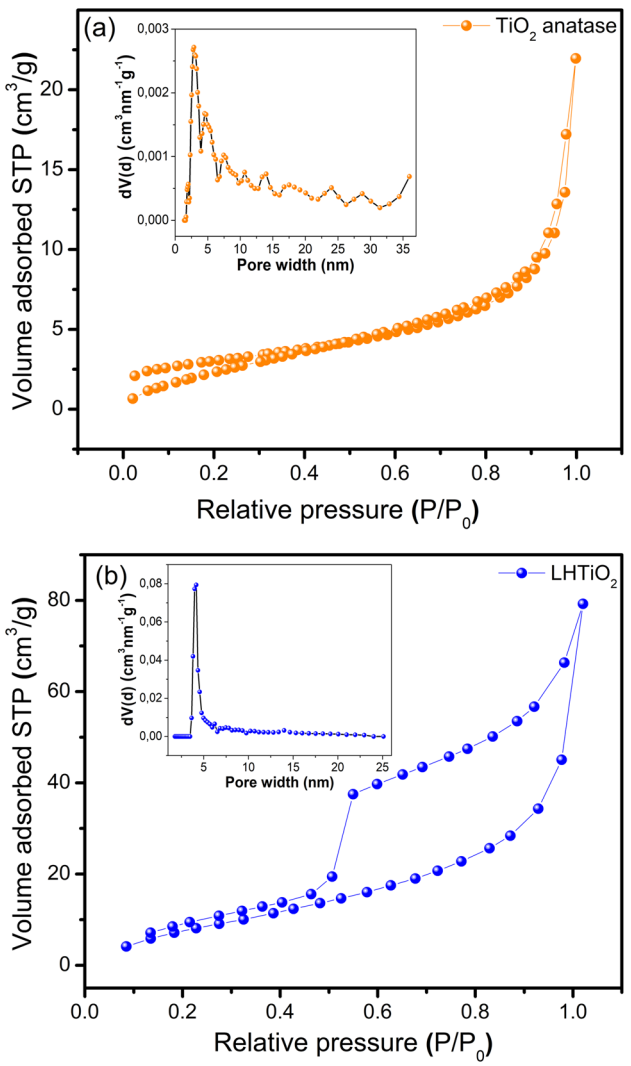

Fig. 5 The nitrogen adsorption/desorption isotherms. The inserts are the pore size distributions for **a** TiO_2 and **b** $LHTiO_2$ composite

for two hours, comparing them with those studied in the absence of any radical scavenger (Fig. 6d). The addition of OA had a slight diminution on the 4-CP degradation efficiency of $LHTiO_2/Cu_2O$. Conversely, the degradation efficiency was significantly reduced in the presence of BQ, indicating that $^{\cdot}O_2^-$ plays a dominant role in the degradation of 4-CP. It was noted that there is a decline in the degradation rate of 4-CP with the introduction of IPA, suggesting that $^{\cdot}OH$ is also an active species in the degradation process, checked by the PL studies with terephthalic acid (TA).

To analyse the charge transfer mechanism, we measured the rates of $^{\cdot}OH$ formation in the samples in aqueous solution under irradiation by PL, using TA as the probe molecule. TA could react with $^{\cdot}OH$ to form highly fluorescent 2-hydroxyterephthalic acid (TAOH). From Fig. 7a, the production rate of radical $^{\cdot}OH$ during irradiation can be easily observed, indicating that the surface of the sample aids in the production of $^{\cdot}OH$ radicals and is favourable to improve photocatalytic activity. The fluorescence intensity at 426 nm significantly improves with increasing irradiation time, demonstrating that $^{\cdot}OH$ radicals form as intermediates of photocatalytic reactions in the degradation of 4-CP [38, 52]. In terms of possible mechanisms, when the sample was illuminated under visible light, in the case of Cu_2O, this perfectly correlates with its bandgap (2.34 eV). For $LHTiO_2$ (3.28 eV), the UV irradiation (~5% of visible light) is sufficient to initiate the semiconductor, producing mobile electrons in the conduction band (CB) and holes in the valence band (VB) [53]. Since the CB of Cu_2O is positioned above the CB of $LHTiO_2$, the electrons photogenerated by Cu_2O should be inserted into the CB of $LHTiO_2$ from the CB of Cu_2O, owing to the potential difference of the band, and the collected electrons on the $LHTiO_2$ CB can convert O_2 to $^{\cdot}O_2^-$, the redox potential (E^o ($O_2/^{\cdot}O_2^-$) = -0.33 V vs NHE)

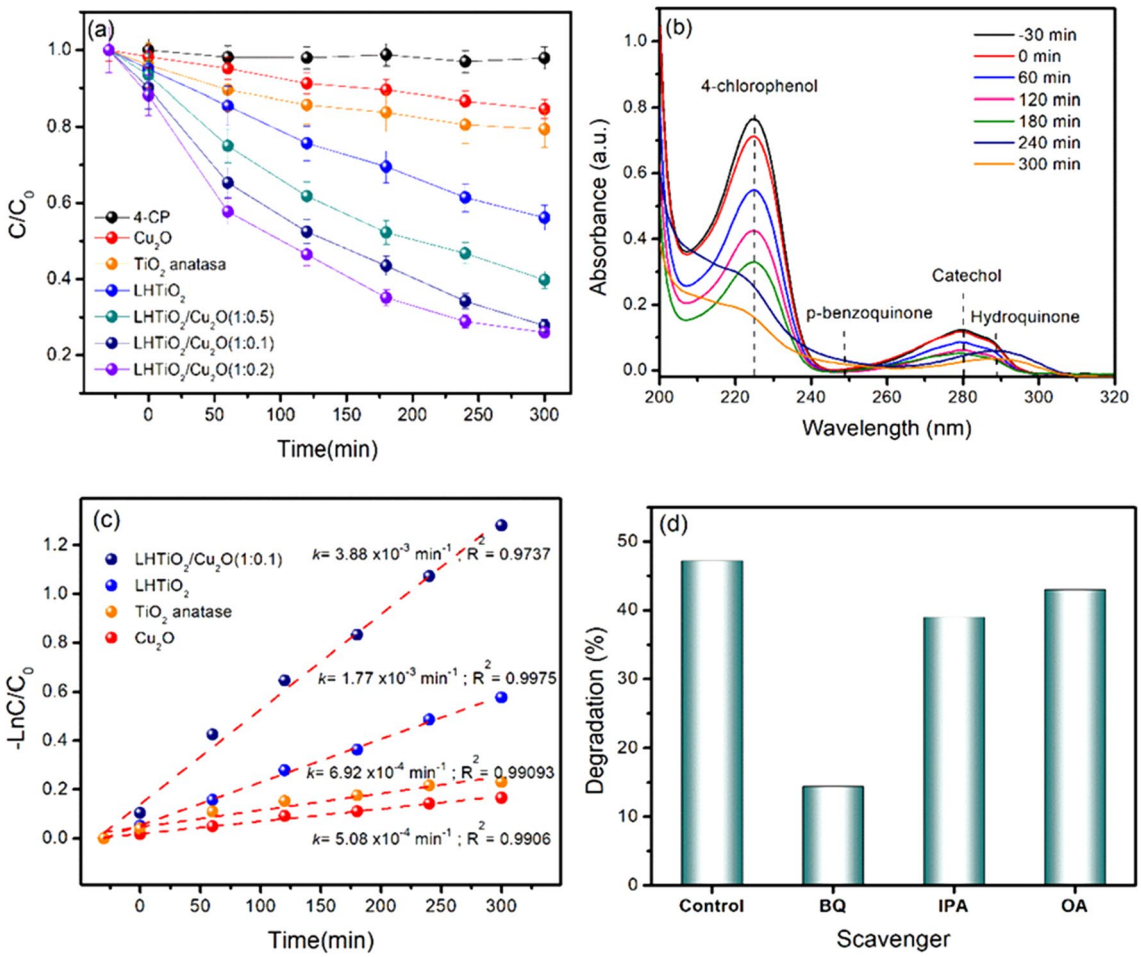

Fig. 6 **a** Photocatalytic performance of samples, **b** UV absorption spectra of the degradation of 4-CP using $LHTiO_2/Cu_2O$ (1:0.1) sample, **c** Photodegradation kinetics of the selected samples for the degradation of 4-CP solution, **d** Photodegradation of $LHTiO_2/Cu_2O$ (1:0.1) in the presence of specific radical scavengers

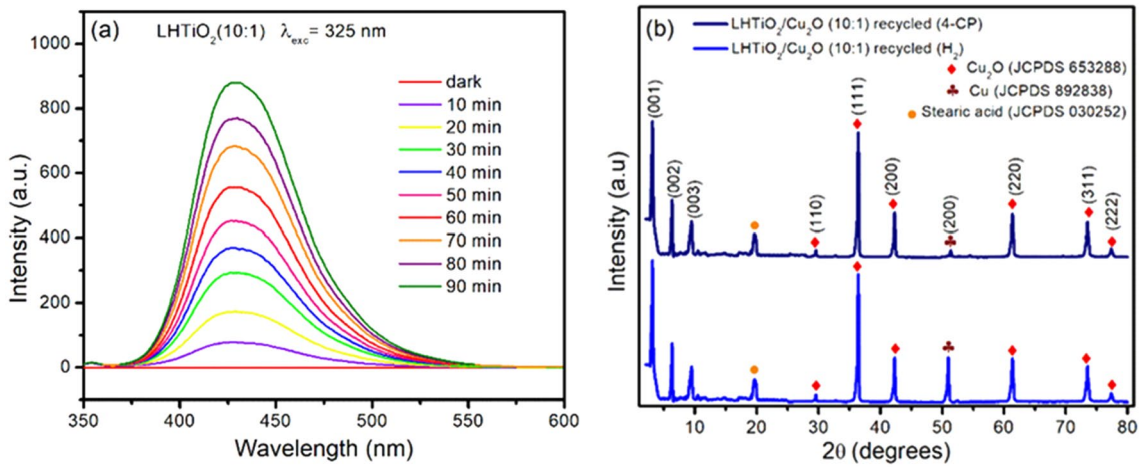

Fig. 7 **a** ˙OH trapping photoluminescence spectra of $LHTiO_2/Cu_2O$ (1:0.1) in a solution of terephthalic acid at room temperature. **b** DRX patterns of samples before and after reuse in photocatalytic degradation and hydrogen evolution

presented in the scheme of the photocatalytic mechanism in Fig. 8. On the other hand, the potential of $LHTiO_2$ photo holes is high, sufficient for water oxidation of hydroxyl groups to hydroxyl radicals ·OH. Meanwhile, the photo holes generated by Cu_2O excitation do not have the energy required for the oxidation of water to hydroxyl radicals (E^o ($H_2O/^{\cdot}OH$) = 2.73 V vs NHE) [54]. Given the experimental results, we proposed that there should be negative charge transfer from energy levels of the CB of $LHTiO_2$ to the BV of Cu_2O, through a type Z-scheme mechanism, to describe the electron transfer processes through the interface in p-n heterojunctions then of the simultaneous excitation of semiconductors. The photogenerated hole in the $LHTiO_2$ unites with the H_2O to produce ·OH, avoiding the recombination of the photogenerated electron–hole formed. Moreover, it should be observed that the charge-carrier movement for the direct Z-scheme photocatalyst is physically feasible, since the migration of photogenerated electrons is valuable due to the electrostatic attraction of the electron and the hole [20, 37, 55]. In addition, we have observed by DRX that after irradiation of the sample (Fig. 7b), the electrons photoexcited cause a partial reduction of Cu_2O to metal Cu. The Cu can additional improve the separation of the charge, acting as a conductive assistance for the mobility of the electronic charge [56] and, impeding recombination in cuprous oxide its main defect [31, 57, 58]. We also tested the recycling of the $LHTiO_2/Cu_2O$ compound (1:0.1) by sampling three times during 120 min of irradiation. The photocatalytic efficiency of $LHTiO_2/Cu_2O$(1:0.1) remained constant until the third cycle, as shown in Fig S5. The recycling indicates the effective reuse of the $LHTiO_2/Cu_2O$ without significant loss in the degradation efficiency.

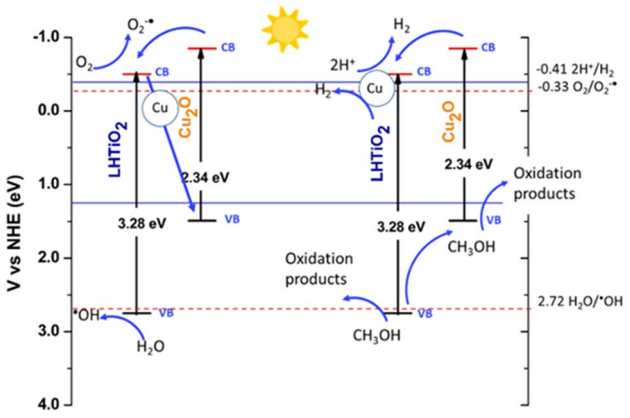

Fig. 8 Scheme of photocatalytic mechanism of the Cu (formed in-situ)/2D $LHTiO_2/Cu_2O$ photocatalysts under sunlight for degradation of 4-CP and the evolution H_2

3.3 Photocatalytic Hydrogen Production

In the present study, the efficiency of H_2 production of the photocatalysts was evaluated using various sacrificial agents. Since one of the crucial factors for the photocatalytic evolution of H_2 is the rapid recombination of pairs of photogenerated electrons, the rapid removal of photogenerated holes through sacrificial hole scavengers in the reaction was observed [59, 60]. The effect of the sacrificial agents was evaluated with formic acid, glucose, sodium sulphite, methanol and glycerol in samples of TiO_2, $LHTiO_2$, $LHTiO_2$ with Cu_2O of 200 nm, and $LHTiO_2$ with Cu_2O of 60 nm, to validate that the role of Cu_2O in photocatalysis is strongly influenced by its particle size [57]. Also, control experiments were carried out to investigate the production of H_2 with only sacrificial reagents under solar irradiation without photocatalysts. The quantities of H_2 produced by the samples in the presence of the selected hole collectors are compared in Fig. 9a.

The results for the $LHTiO_2/Cu_2O$(60 nm) composite showed a significantly higher volume of H_2 evolved in the presence of methanol, followed by glycerol and 1 M sodium sulphite. The best results were always obtained for methanol as a sacrificing reagent in the photocatalytic evolution of H_2 from aqueous solutions. This can be mainly attributed to its ability to produce an electron donor in the conduction band, preventing their recombination and increasing the potential for the evolution of H_2 [43, 61].

The hydrogen evolution reactions were performed using different photocatalyst ratios to estimate which ratio has the best efficiency for hydrogen evolution. Figure 9b shows the hydrogen evolution over time in the presence of $LHTiO_2/Cu_2O$ composites with $LHTiO_2$ molar ratios of 1:0.05, 1:0.1, and 1:0.2. For all samples, the amount of produced H_2 increased with irradiation time. The optimal photocatalytic hydrogen generation rate, achieved with the $LHTiO_2/Cu_2O$ (1:0.1) composite, was 20.34 mmol g^{-1} h^{-1}, which was about 2 orders of magnitude higher than that of the composite $LHTiO_2$ catalyst (10.4 mmol g^{-1} h^{-1}) and 2.7 times higher than the TiO_2 anatase (7.58 mmol g^{-1} h^{-1}). Recently, similar rates of H_2 evolution for heterostructured systems of TiO_2 with Cu_2O (16.00 mmol g^{-1} h^{-1} and 24.83 mmol g^{-1} h^{-1}) [13, 33] have been reported.

3.4 Mechanism of Hydrogen Production

The possible mechanism proposed for the evolution of hydrogen from an aqueous methanol solution using $LHTiO_2/Cu_2O$ is shown in the Fig. 8. Under photoirradiation, $LHTiO_2$ and Cu_2O separately generate electron–hole pairs at CB and VB, respectively. Despite the conduction band potentials of $LHTiO_2$ and Cu_2O being more negative than the reduction potential of $2H^+/H_2$, the rate of H_2

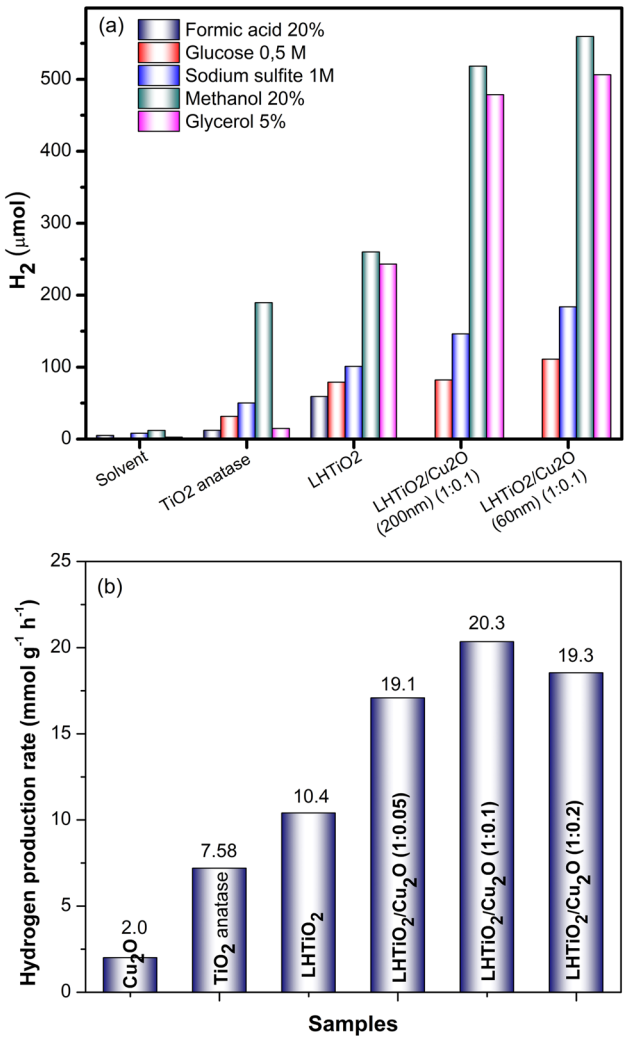

Fig. 9 **a** Effect of the sacrificial agents evaluated with formic acid, glucose, sodium sulphite, methanol, and glycerol in samples and **b** Hydrogen evolution of samples in methanol

evolution was fairly low due to the rapid recombination of photo-excited electron–hole pairs. Alternatively, for the $LHTiO_2/Cu_2O$ composite under visible light, both $LHTiO_2$ and Cu_2O are photoexcited to produce electrons and holes, in the acoupling of semiconductors p-n. Thus, the enhanced activity can be asignated to the fact an internal electrical field is produced in the interface which improves the electron–hole separation efficiency as compared to $LHTiO_2$. In the $LHTiO_2/Cu_2O$, the CB photogenerated electrons of Cu_2O should be inserted into the CB of $LHTiO_2$, due to the potential band difference between semiconductors, and react fast with protons producing hydrogen. Furthermore, sacrificial agents (water/methanol) are consumed by photogenerated holes in the VB of Cu_2O and $LHTiO_2$, facilitating the charge separation and transfer during the photoexcitation process, which aids the improvement of H_2 production [31, 43]. We have observed, by DRX, the presence of Cu after irradiation (Fig. 7b), which would provide additional sites for the reduction reaction with protons, favouring the evolution of hydrogen, and additionally, the Cu could limit the problem of self-oxidation to Cu_2O [58, 62]. Through the results obtained, we proposed a type II mechanism band alignment, formed between $LHTiO_2$ and Cu_2O. Therefore, the formation of the p-n heterojunction of $LHTiO_2/Cu_2O$ suppresses load recombination, improving the photocatalytic activity (Fig. 9) [63, 64].

The recycling study was carried out to evaluate the stability of the photocatalyst $LHTiO_2/Cu_2O$ (1:0.1) in a 20% aqueous solution of methanol. Each cycle was maintained for 2.5 h, and at the beginning of the second and third cycles, 3 mL of methanol was added. After each cycle, the system was left for 24 h, tightly sealed with vacuum and N_2. Fig. S6 shows the results of the recycled $LHTiO_2/Cu_2O$ composite, up to 7 h. To verify the structure of $LHTiO_2/Cu_2O$ (1:0.1), the recycled sample was measured by XRD. The results of XRD patterns indicated that the characteristic diffraction peaks of $LHTiO_2/Cu_2O$ and the diffraction peaks of metallic Cu are maintained. According to the results obtained, the prolonged activity in the photocatalytic process retains the coexistence of Cu and Cu_2O in the reaction.

3.5 Electrochemical Measurement

To confirm the behaviour of the photocurrent response concerning the dynamics of charge transfer and percentage of recombination at the $LHTiO_2/Cu_2O$/electrolyte interface, for individual and combined systems, potential pulse measurements were made under constant illumination, following the methodology described by L.M. Peter [65]. Figure 10 represents the photocurrent response of Cu_2O, $LHTiO_2$, and $LHTiO_2/Cu_2O$, respectively, at a 0 V bias versus Ag/AgCl reference electrode with a pulse of 20 s under intermittent irradiation LED $\lambda = 365$ nm (50 W m^{-2}), in a 0.5 M solution of Na_2SO_4.

For all systems, an increase is seen in the steady-state photocurrent response, which is the sum of the currents recorded during the lighting of the electrodes, added to the effect of the curvature of the bands down and the bulk of the semiconductor, promoting the migration of photogenerated carriers (e^-/h^+). In addition, the response in photocurrent increases for all systems, following the same efficiency pattern that was registered for the degradation and hydrogen photogeneration process: $LHTiO_2/Cu_2O > LHTiO_2 > Cu_2O$, which also corroborates with the order of catalytic efficiency of all the samples. In general, the relationship between initial photocurrent (j_0) and the stationary photocurrent (j_1) is very close in all cases to the unit. Therefore, the recombination rates for Cu_2O, $LHTiO_2$ and the $LHTiO_2/Cu_2O$ systems are low [66].

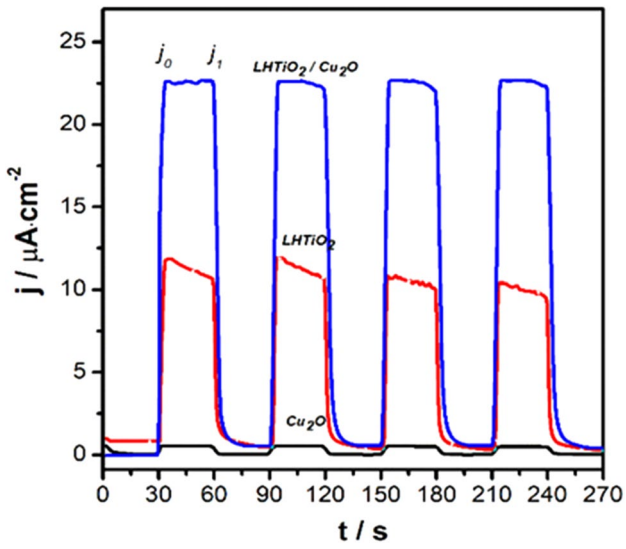

Fig. 10 Photocurrent transients for electrodes (black line) Cu_2O, (red line) $LHTiO_2$, (blue line) $LHTiO_2/Cu_2O$. Photocurrent pulses were realized in 0.5 M Na_2SO_4 using an LED $\lambda = 365$ nm (50 W m^{-2})

The interfacial charge transfer processes occurring at the semiconductor-electrolyte interfaces have been investigated using EIS and PEIS [67].

Figure 11a and b represent the EIS and PEIS Nyquist plots of the samples Cu_2O, $LHTiO_2$, and $LHTiO_2/Cu_2O$, respectively. In the Nyquist plots for EIS, it is observed that the arc of the semicircles decreases at low frequencies ($Cu_2O < LHTiO_2/Cu_2O < LHTiO_2$) according to the relationship between the decrease in electrical resistivity (Cu_2O 1.6×10^4 Ω cm [68], TiO_2 2.34×10^4 Ω cm [69]) and the acceleration of the interfacial transfer processes, recorded by EIS measurements [70].

Figure 11b shows only one semicircle in the Nyquist plot under illumination (PEIS) for the three electrodes, which is associated with the processes of charge transfer in the semiconductor space charge zone and the electrified interfaces [71]. The decrease of the semicircle arc diameter in the Nyquist plots under illumination ($LHTiO_2/Cu_2O > LHTiO_2 > Cu_2O$) correlates with the most effective separation of the photogenerated charge carriers (e^-, h^+) and, therefore, accelerates the charge transfer across the photoelectrode/solution interface [72].

The inset in Fig. 11b, is the equivalent circuit diagram used in the simulation, considering the charge transfer across the semiconductor/electrolyte interface. Rs corresponds to the resistance of the solution. The resistance to load transfer in the double layer is represented by Rdl, while CPEdl corresponds to the load of the double layer. The Rct // CPEsc configuration describes the resistance to load transfer from the semiconductor and the capacitance of the semiconductor space charge zone, both components associated with the processes of transmission of charge carriers, as well as the separation and recombination of pairs e^-/h^+. The substitution of the capacitive components of the circuit by constant phase elements (CPE) was carried out considering that the systems analysed have a heterogeneous structure and high microscopic roughness, which leads to a non-ideal capacitance, associated with a non-uniform distribution of the current [73]. Rct decreases significantly upon illumination for all photoelectrodes (EIS-Rct: Cu_2O 8.663 kΩ cm^{-2}, $LHTiO_2$ 18.051 kΩ cm^{-2}, $LHTiO_2/Cu_2O$ 10.727 kΩ cm^{-2}, and PEIS-Rct: Cu_2O 5.681 kΩ cm^{-2}, $LHTiO_2$ 4.215 kΩ cm^{-2}, $LHTiO_2/Cu_2O$ 2.201 kΩ cm^{-2}), indicating that illumination greatly accelerates the charge transfer reaction at the semiconductor/solution interface due to the photoinduced increase of carrier density. The variation trend of Rct with $LHTiO_2/Cu_2O$ composite agrees well with that of the photocurrent density and the smallest Rct value, both in the dark and under illumination, suggesting that the $LHTiO_2/Cu_2O$ composite accelerates the charge transfer across the semiconductor/solution interface, which explains the good photocatalytic performance of the compound.

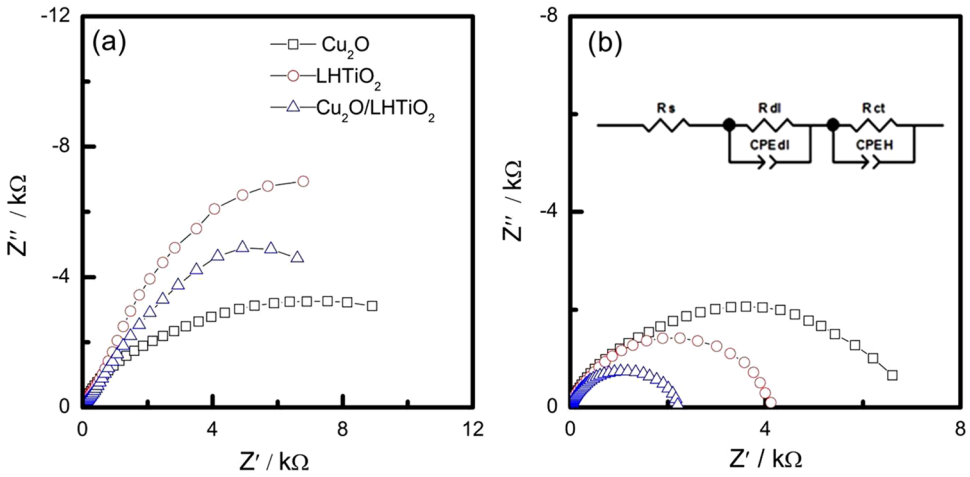

Fig. 11 **a** EIS and **b** PEIS spectra for electrodes (open square) Cu_2O, (open circle) $LHTiO_2$, (open triangle) $LHTiO_2/Cu_2O$. The insert corresponds to the equivalent circuit used in the simulation, considering the electrode and the dissolution interface

4 Conclusion

The formation of a novel photocatalyst of 2D-TiO_2 in layers of a sheets-like arrangement with Cu_2O nanoparticles was prepared and characterized using various techniques. The results indicated that the synergy between the semiconductors generated the separation of electrons and photogenerated holes and exhibited an improved visible light absorption, demonstrating the clear contribution of Cu_2O and the 2D structure of $LHTiO_2$ in the photocatalytic efficiency of the compound for degradation of 4-chlorophenol and hydrogen evolution. Photoinduced charge separation mechanisms, a Z-scheme for photocatalytic degradation, and a type II heterojunction to evolution photocatalytic hydrogen are proposed. The recyclability experiments showed that the photocatalysts could be reused for at least three cycles without a significant change in their activity.

The photoelectrochemical evaluation corroborates the order of catalytic efficiency of all the samples, showing that the compound $LHTiO_2/Cu_2O$ exhibits an improved visible light absorption with low recombination rates and an effective separation and charge transfer efficient carriers photogenerated in photocatalytic reactions.

Acknowledgements This work was supported by Project funded by the Research Continuity Project Fund, year 2019, code LPC19-01, Universidad Tecnologica Metropolitana, Universidad de Chile, FONDECYT 1171803, CMST Spanish MINECO projects PHENTOM (FIS2015-70862-P) and Severo Ochoa (SEV-2013-0295) and the CERCA Programme/Generalitat de Catalunya, Programa Fondequip XPS EQM 140044 and SEM EQM 150101. We want to thank Dra. Marjorie Segovia for the help in the samples preparation of nanoparticles Cu_2O.

Compliance with Ethical Standards

Conflicts of interest The authors have no conflicts of interest.

Research Involving Human and/or Animal Rights There were no human or animal subjects involved in this research.

References

1. Xu C, Ravi Anusuyadevi P, Aymonier C et al (2019) Nanostructured materials for photocatalysis. Chem Soc Rev 48:3868–3902. https://doi.org/10.1039/c9cs00102f
2. Luo J, Zhang S, Sun M et al (2019) A critical review on energy conversion and environmental remediation of photocatalysts with remodeling crystal lattice, surface, and interface. ACS Nano 13:9811–9840. https://doi.org/10.1021/acsnano.9b03649
3. Wang Q, Domen K (2020) Particulate photocatalysts for light-driven water splitting: mechanisms, challenges, and design strategies. Chem Rev 120:919–985. https://doi.org/10.1021/acs.chemrev.9b00201
4. Zhang L, Ran J, Qiao S-Z, Jaroniec M (2019) Characterization of semiconductor photocatalysts. Chem Soc Rev 48:5184–5206. https://doi.org/10.1039/c9cs00172g
5. Wu H, Tan HL, Toe CY et al (2020) Photocatalytic and photoelectrochemical systems: similarities and differences. Adv Mater 32:1904717. https://doi.org/10.1002/adma.201904717
6. Li D, Yu JCC, Nguyen VH et al (2018) A dual-function photocatalytic system for simultaneous separating hydrogen from water splitting and photocatalytic degradation of phenol in a twin-reactor. Appl Catal B Environ 239:268–279. https://doi.org/10.1016/j.apcatb.2018.08.010
7. Nakata K, Fujishima A (2012) TiO_2 photocatalysis: design and applications. J Photochem Photobiol C Photochem Rev 13:169–189. https://doi.org/10.1016/j.jphotochemrev.2012.06.001
8. Kim J, Monllor-Satoca D, Choi W (2012) Simultaneous production of hydrogen with the degradation of organic pollutants using TiO_2 photocatalyst modified with dual surface components. Energy Environ Sci 5:7647–7656. https://doi.org/10.1039/c2ee21310a
9. Riente P, Noël T (2019) Application of metal oxide semiconductors in light-driven organic transformations. Catal Sci Technol 9:5186–5232. https://doi.org/10.1039/c9cy01170f
10. Nasr M, Eid C, Habchi R et al (2018) Recent progress on titanium dioxide nanomaterials for photocatalytic applications. Chemsuschem 11:3023–3047. https://doi.org/10.1002/cssc.201800874
11. Hu Z, Wang X, Dong H et al (2017) Efficient photocatalytic degradation of tetrabromodiphenyl ethers and simultaneous hydrogen production by TiO_2-Cu_2O composite films in N_2 atmosphere: influencing factors, kinetics and mechanism. J Hazard Mater 340:1–15. https://doi.org/10.1016/j.jhazmat.2017.07.009
12. Wei T, Zhu Y-N, An X et al (2019) Defect modulation of Z-scheme TiO_2/Cu_2O photocatalysts for durable water splitting. ACS Catal 9:8346–8354. https://doi.org/10.1021/acscatal.9b01786
13. Trang TNQ, Tu LTN, Man TV et al (2019) A high-efficiency photoelectrochemistry of Cu_2O/TiO_2 nanotubes based composite for hydrogen evolution under sunlight. Compos Part B Eng 174:106969. https://doi.org/10.1016/j.compositesb.2019.106969
14. Cheng WY, Yu TH, Chao KJ, Lu SY (2014) Cu_2O-decorated mesoporous TiO_2 beads as a highly efficient photocatalyst for hydrogen production. ChemCatChem 6:293–300. https://doi.org/10.1002/cctc.201300681
15. Uddin MT, Babot O, Thomas L et al (2015) New insights into the photocatalytic properties of RuO_2/TiO_2 mesoporous heterostructures for hydrogen production and organic pollutant photodecomposition. J Phys Chem C 119:7006–7015. https://doi.org/10.1021/jp512769u
16. Benavente E, Maldonado C, Devis S et al (2016) A hybrid organic-inorganic layered TiO_2 based nanocomposite for sunlight photocatalysis. RSC Adv 6:18538–18541. https://doi.org/10.1039/c5ra26981d
17. Liu S, Zhang N, Tang ZR, Xu YJ (2012) Synthesis of one-dimensional CdS@TiO_2 core-shell nanocomposites photocatalyst for selective redox: the dual role of TiO_2 shell. ACS Appl Mater Interfaces 4:6378–6385. https://doi.org/10.1021/am302074p
18. Peng W, Li Y, Zhang F et al (2017) Roles of two-dimensional transition metal dichalcogenides as cocatalysts in photocatalytic hydrogen evolution and environmental remediation. Ind Eng Chem Res 56:4611–4626. https://doi.org/10.1021/acs.iecr.7b00371
19. Tsai CE, Yeh SM, Chen CH, Lin HN (2019) Flexible photocatalytic paper with Cu_2O and Ag nanoparticle-decorated ZnO nanorods for visible light photodegradation of organic dye. Nanoscale Res Lett. https://doi.org/10.1186/s11671-019-3034-7
20. Ye F, Su Y, Quan X et al (2019) Constructing desired interfacial energy band alignment of Z-scheme TiO_2-Pd-Cu_2O hybrid by controlling the contact facet for improved photocatalytic performance. Appl Catal B Environ 244:347–355. https://doi.org/10.1016/j.apcatb.2018.10.066

21. Liao Y, Deng P, Wang X et al (2018) A facile method for preparation of Cu_2O-TiO_2 NTA heterojunction with visible-photocatalytic activity. Nanoscale Res Lett. https://doi.org/10.1186/s11671-018-2637-8
22. Zheng Z, Huang B, Wang Z et al (2009) Crystal faces of Cu_2O and their stabilities in photocatalytic reactions. J Phys Chem C 113:14448–14453. https://doi.org/10.1021/jp904198d
23. Sinatra L, Lagrow AP, Peng W et al (2015) A Au/Cu_2O-TiO_2 system for photo-catalytic hydrogen production. A pn-junction effect or a simple case of in situ reduction? J Catal 322:109–117. https://doi.org/10.1016/j.jcat.2014.11.012
24. Tamiolakis I, Papadas IT, Spyridopoulos KC, Armatas GS (2016) Mesoporous assembled structures of Cu_2O and TiO_2 nanoparticles for highly efficient photocatalytic hydrogen generation from water. RSC Adv 6:54848–54855. https://doi.org/10.1039/c6ra08546f
25. Chu S, Zheng X, Kong F et al (2011) Architecture of Cu_2O@TiO_2 core-shell heterojunction and photodegradation for 4-nitrophenol under simulated sunlight irradiation. Mater Chem Phys 129:1184–1188. https://doi.org/10.1016/j.matchemphys.2011.06.004
26. Surikanti GR, Bandarapu AK, Sunkara MV (2019) A facile one pot synthesis of Cu_2O@TiO_2: a nanocomposite catalyst for enhanced visible light driven photocatalysis #. ChemistrySelect 4:2249–2257. https://doi.org/10.1002/slct.201900003
27. Ding RC, Fan YZ, Wang GS (2018) High efficient Cu_2O/TiO_2 nanocomposite photocatalyst to degrade organic pollutant under visible light irradiation. Chem Select 3:1682–1687. https://doi.org/10.1002/slct.201702650
28. Liu J, Wen M, Chen H et al (2014) Assembly of TiO_2-on-Cu_2O nanocubes with narrow-band Cu_2O-induced visible-light-enhanced photocatalytic activity. ChemPlusChem 79:298–303. https://doi.org/10.1002/cplu.201300278
29. Aguirre ME, Zhou R, Eugene AJ et al (2017) Cu_2O/TiO_2 heterostructures for CO_2 reduction through a direct Z-scheme: protecting Cu_2O from photocorrosion. Appl Catal B Environ 217:485–493. https://doi.org/10.1016/j.apcatb.2017.05.058
30. Xu H, Ouyang S, Liu L et al (2014) Porous-structured Cu_2O/TiO_2 nanojunction material toward efficient CO_2 photoreduction. Nanotechnology. https://doi.org/10.1088/0957-4484/25/16/165402
31. Xi Z, Li C, Zhang L et al (2014) Synergistic effect of Cu_2O/TiO_2 heterostructure nanoparticle and its high H_2 evolution activity. Int J Hydrogen Energy 39:6345–6353. https://doi.org/10.1016/j.ijhydene.2014.01.209
32. Zhang YH, Li YL, Jiu BB et al (2019) Highly enhanced photocatalytic H_2 evolution of Cu_2O microcube by coupling with TiO_2 nanoparticles. Nanotechnology. https://doi.org/10.1088/1361-6528/aafccb
33. Li G, Huang J, Chen J et al (2019) Highly active photocatalyst of Cu_2O/TiO_2 octahedron for hydrogen generation. ACS Omega 4:3392–3397. https://doi.org/10.1021/acsomega.8b03404
34. Zeghioud H, Assadi AA, Khellaf N et al (2019) Photocatalytic performance of Cu_xO/TiO_2 deposited by HiPIMS on polyester under visible light LEDs: oxidants, ions effect, and reactive oxygen species investigation. Materials (Basel) 12:412. https://doi.org/10.3390/ma12030412
35. Ibrahim MM, Mezni A, El-Sheshtawy HS et al (2019) Direct Z-scheme of Cu_2O/TiO_2 enhanced self-cleaning, antibacterial activity, and UV protection of cotton fiber under sunlight. Appl Surf Sci 479:953–962. https://doi.org/10.1016/j.apsusc.2019.02.169
36. Li H, Zhong J, Zhu H et al (2019) Hybrid Cu_2O/TiO_2 nanocomposites with enhanced photocatalytic antibacterial activity toward acinetobacter Baumannii. ACS Appl Bio Mater 2:4892–4903. https://doi.org/10.1021/acsabm.9b00644
37. Segovia M, Alegría M, Aliaga J et al (2019) Heterostructured 2D ZnO hybrid nanocomposites sensitized with cubic Cu_2O nanoparticles for sunlight photocatalysis. J Mater Sci 54:13523–13536. https://doi.org/10.1007/s10853-019-03878-x
38. Bubacz K, Kusiak-Nejman E, Tryba B, Morawski AW (2013) Investigation of OH radicals formation on the surface of TiO_2/N photocatalyst at the presence of terephthalic acid solution. Estimation of optimal conditions. J Photochem Photobiol A Chem. https://doi.org/10.1016/j.jphotochem.2013.04.003
39. Tauc J, Menth A (1972) States in the gap. J Non Cryst Solids 8–10:569–585. https://doi.org/10.1016/0022-3093(72)90194-9
40. Murphy AB (2007) Band-gap determination from diffuse reflectance measurements of semiconductor films, and application to photoelectrochemical water-splitting. Sol Energy Mater Sol Cells 91:1326–1337. https://doi.org/10.1016/j.solmat.2007.05.005
41. Cheng Y, Gao X, Zhang X et al (2018) Synthesis of a TiO_2-Cu_2O composite catalyst with enhanced visible light photocatalytic activity for gas-phase toluene. New J Chem 42:9252–9259. https://doi.org/10.1039/c8nj00409a
42. Mathew S, Kumar Prasad A, Benoy T et al (2012) UV-visible photoluminescence of TiO_2 nanoparticles prepared by hydrothermal method. J Fluoresc 22:1563–1569. https://doi.org/10.1007/s10895-012-1096-3
43. Praveen Kumar D, Lakshmana Reddy N, Srinivas B et al (2016) Stable and active Cu_xO/TiO_2 nanostructured catalyst for proficient hydrogen production under solar light irradiation. Sol Energy Mater Sol Cells 146:63–71. https://doi.org/10.1016/j.solmat.2015.11.030
44. Lalitha K, Sadanandam G, Kumari VD et al (2010) Highly stabilized and finely dispersed Cu_2O/TiO_2: a promising visible sensitive photocatalyst for continuous production of hydrogen from glycerol:water mixtures. J Phys Chem C 114:22181–22189. https://doi.org/10.1021/jp107405u
45. Greczynski G, Hultman L (2020) X-ray photoelectron spectroscopy: towards reliable binding energy referencing. Prog Mater Sci 107:100591. https://doi.org/10.1016/j.pmatsci.2019.100591
46. Greczynski G, Hultman L (2017) C 1s peak of adventitious carbon aligns to the vacuum level: dire consequences for material's bonding assignment by photoelectron spectroscopy. ChemPhysChem. https://doi.org/10.1002/cphc.201700126
47. Nava-Núñez MY, Jimenez-Relinque E, Grande M et al (2020) Photocatalytic BiO_X mortars under visible light irradiation: compatibility, Nox efficiency and nitrate selectivity. Catalysts 10:226. https://doi.org/10.3390/catal10020226
48. Thommes M, Kaneko K, Neimark AV et al (2015) Physisorption of gases, with special reference to the evaluation of surface area and pore size distribution (IUPAC Technical Report). Pure Appl Chem 87:1051–1069. https://doi.org/10.1515/pac-2014-1117
49. Zhang J, Yu J, Zhang Y et al (2011) Visible light photocatalytic H2-production activity of CuS/ZnS porous nanosheets based on photoinduced interfacial charge transfer. Nano Lett 11:4774–4779. https://doi.org/10.1021/nl202587b
50. Castañeda C, Tzompantzi F, Gómez R, Rojas H (2016) Enhanced photocatalytic degradation of 4-chlorophenol and 2,4-dichlorophenol on in situ phosphated sol-gel TiO_2. J Chem Technol Biotechnol 91:2170–2178. https://doi.org/10.1002/jctb.4943
51. Liu W, Wang M, Xu C et al (2013) Ag_3PO_4/ZnO: An efficient visible-light-sensitized composite with its application in photocatalytic degradation of Rhodamine B. Mater Res Bull 48:106–113. https://doi.org/10.1016/j.materresbull.2012.10.015
52. Qu X, Kirschenbaum LJ, Borish ET (2000) Hydroxyterephthalate as a fluorescent probe for hydroxyl radicals: application to hair melanin. Photochem Photobiol 71:307–313. https://doi.org/10.1562/0031-8655(2000)0710307haafpf2.0.co2
53. Youssef Z, Colombeau L, Yesmurzayeva N et al (2018) Dye-sensitized nanoparticles for heterogeneous photocatalysis: cases studies with TiO_2, ZnO, fullerene and graphene for water

purification. Dye Pigment 159:49–71. https://doi.org/10.1016/j.dyepig.2018.06.002
54. Wardman P (1989) Reduction potentials of one electron couples involving free radicals in aqueous solution. J Phys Chem Ref Data 18:1637–1755. https://doi.org/10.1063/1.555843
55. Low J, Jiang C, Cheng B et al (2017) A review of direct Z-scheme photocatalysts. Small Methods 1:1700080. https://doi.org/10.1002/smtd.201700080
56. Das D, Makal P (2020) Narrow band gap reduced TiO_2-B: Cu nanowire heterostructures for efficient visible light absorption, charge separation and photocatalytic degradation. Appl Surf Sci 506:144880. https://doi.org/10.1016/j.apsusc.2019.144880
57. Li L, Xu L, Shi W, Guan J (2013) Facile preparation and size-dependent photocatalytic activity of Cu_2O nanocrystals modified titania for hydrogen evolution. Int J Hydrogen Energy 38:816–822. https://doi.org/10.1016/j.ijhydene.2012.10.064
58. Janczarek M, Endo M, Zhang D, Wang K, Kowalska E (2018) Enhanced photocatalytic and antimicrobial performance of cuprous oxide/titania: the effect of titania matrix. Materials (Basel) 11:2069. https://doi.org/10.3390/ma11112069
59. Denisov N, Yoo JE, Schmuki P (2019) Effect of different hole scavengers on the photoelectrochemical properties and photocatalytic hydrogen evolution performance of pristine and Pt-decorated TiO_2 nanotubes. Electrochim Acta 319:61–71. https://doi.org/10.1016/j.electacta.2019.06.173
60. Sreethawong T, Puangpetch T, Chavadej S, Yoshikawa S (2007) Quantifying influence of operational parameters on photocatalytic H_2 evolution over Pt-loaded nanocrystalline mesoporous TiO_2 prepared by single-step sol-gel process with surfactant template. J Power Sources 165:861–869. https://doi.org/10.1016/j.jpowsour.2006.12.050
61. Guzman F, Chuang SSC, Yang C (2013) Role of methanol sacrificing reagent in the photocatalytic evolution of hydrogen. Ind Eng Chem Res 52:61–65. https://doi.org/10.1021/ie301177s
62. Zhen W, Jiao W, Wu Y et al (2017) The role of a metallic copper interlayer during visible photocatalytic hydrogen generation over a $Cu/Cu_2O/Cu/TiO_2$ catalyst. Catal Sci Technol 7:5028–5037. https://doi.org/10.1039/c7cy01432e
63. Haque F, Daeneke T, Kalantar-zadeh K, Ou JZ (2018) Two-dimensional transition metal oxide and chalcogenide-based photocatalysts. Nano-Micro Lett 10:1–27. https://doi.org/10.1007/s40820-017-0176-y
64. Ida S, Takashiba A, Koga S et al (2014) Potential gradient and photocatalytic activity of an ultrathin p-n junction surface prepared with two-dimensional semiconducting nanocrystals. J Am Chem Soc 136:1872–1878. https://doi.org/10.1021/ja409465k
65. Peter LM (2013) Energetics and kinetics of light-driven oxygen evolution at semiconductor electrodes: the example of hematite. J Solid State Electrochem 550:315–326. https://doi.org/10.1007/s10008-012-1957-3
66. Yang L, Wang W, Zhang H et al (2017) Electrodeposited Cu_2O on the 101 facets of TiO_2 nanosheet arrays and their enhanced photoelectrochemical performance. Sol Energy Mater Sol Cells 165:27–35. https://doi.org/10.1016/j.solmat.2017.02.026
67. Yu D, Yu D, Dai J et al (2020) Growth of Cu_2O/TiO_2 heterojunction and its photoelectrochemical properties. Mater Lett 263:1–4. https://doi.org/10.1016/j.matlet.2019.127225
68. Niveditha CV, JabeenFatima MJ, Sindhu S (2016) Electrochemical synthesis of p-type copper oxides. Nanosyst Phys Chem Math 7:747–751
69. Senain I, Nayan N, Saim H (2010) Structural and electrical properties of TiO_2 thin film derived from sol-gel method using titanium (IV) butoxide. Int J Integr Eng 4:29–35
70. Szaniawska E, Bienkowski K, Rutkowska IA et al (2018) Enhanced photoelectrochemical CO_2-reduction system based on mixed Cu_2O–nonstoichiometric TiO_2 photocathode. Catal Today 300:145–151. https://doi.org/10.1016/j.cattod.2017.05.099
71. Santamaria M, Conigliaro G, Di Franco F, Di Quarto F (2014) Photoelectrochemical evidence of Cu_2O/TiO_2nanotubes heterojunctions formation and their physicochemical characterization. Electrochim Acta 144:315–323. https://doi.org/10.1016/j.electacta.2014.07.154
72. Yin H, Wang X, Wang L et al (2015) Cu_2O/TiO_2 heterostructured hollow sphere with enhanced visible light photocatalytic activity. Mater Res Bull 72:176–183. https://doi.org/10.1016/j.materresbull.2015.07.030
73. Oh JT, Chowdhury SR, Lee II T, Misra M (2019) Synergetic influence of Au/Cu_2O core-shells nanoparticle on optical, photoelectrochemical, and catalytic activities of $Au/Cu_2O/TiO_2$ nanocomposite. Dye Pigment 160:936–943. https://doi.org/10.1016/j.dyepig.2018.09.003